CrossMark

A simplified stability analysis method for LV inverter-based microgrids

Bülent DAĞ[1] , **M. Timur AYDEMIR**[2]

MPCE

Abstract This paper presents a simplified small-signal stability analysis method for low voltage (LV) inverter-based microgrids, in a generalized manner. The simplification is based on a simplified microgrid structure that relies on dominating inverter coupling impedances with respect to interconnecting line impedances of LV distribution networks. The analysis is further simplified by analytically determining equilibrium points of system state variables in terms of known microgrid parameters. And it eliminates the additional analysis required for determination of the equilibrium points of the state variables. Simulation and analysis results show that the proposed method successfully predicts the instability boundaries of microgrid systems for resistive interconnecting lines.

✉ Bülent DAĞ
   bulent.dag@tubitak.gov.tr

   M. Timur AYDEMIR
   aydemirmt@gazi.edu.tr

[1] Space Technologies Research Institute, TUBITAK, Ankara, Turkey

[2] Gazi University Electrical and Electronics Engineering Department, Ankara, Turkey

STATE GRID
STATE GRID ELECTRIC POWER RESEARCH INSTITUTE

1 Introduction

Microgrid has emerged recently as a promising low voltage (LV) electrical network application in smart grids as an alternative to the conventional centralized structure. In grid connected mode, microgrid behaves as a controllable single unit by appropriate supervisory control techniques. It provides control and operation flexibility to the distributed generation networks including renewable sources [1]. Islanded operation of microgrids, on the other hand, requires decentralized local control techniques as in conventional networks for reliable network operation. In this mode, droop based voltage and frequency controls are commonly applied to distributed generator (DG) inverters [2–7].

For such nonlinear systems, small-signal model of the system is widely used to observe the effect of system parameters on stability under small disturbances [8]. However, complete dynamic model of microgrids is quite complicated due to multi-control stages of DG inverters [9, 10]. As the number of inverters increases in the microgrid, the analysis becomes quite a difficult procedure. Therefore, the recent trend is the simplification of the dynamical model of microgrids and developing a generalized analysis method. The microgrid model proposed in [11] simplifies the analysis by neglecting voltage and current dynamics of DG inverters in the microgrid. However, as shown in [12], this model loses accuracy in the instability boundaries due to static modelling of interconnecting line impedances. To overcome this drawback, a dynamic phasors based modelling has been proposed in [12]. However, the model considers only a single droop controlled DG inverter connected to a stiff (constant voltage) AC network. A more detailed microgrid model, including line currents as state variables, has been proposed in [13]. However, the model neglects power filters of DGs, and considers a microgrid structure without coupling impedances at DG

outputs by assuming large enough interconnecting line impedances in the microgrid. Apparently this model is not suitable for LV networks with small interconnecting line impedances. Besides, power filters are required in practice to filter out harmonics and to damp frequency and voltage variations. A generalized stability analysis method for ring type microgrid structures has been proposed in [14], considering only power stage dynamics. However, too many assumptions in the proposed microgrid model reduce the accuracy of the method. Most recently, singular perturbation based model reductions have been presented in [15–17], which detect the fast states of the system and reduce them from the model. These models have a variety of accuracy levels depending on the order of the reduction.

On the other hand, since all of the microgrid models mentioned above are linearized small-signal dynamic models, they require additional analysis to determine initial conditions of state variables. As a common approach, load flow analysis tools or dynamic simulations (for small scale microgrids) are used to obtain equilibrium points of the state variables, which makes the stability analysis quite challenging as the microgrid enlarges.

This paper proposes a simplified and generalized stability analysis method to facilitate the analysis and parameter selection for microgrids. Firstly, we propose a common LV microgrid network model, based on the assumption of weak line impedances of LV distribution networks with respect to coupling impedances of DGs. Then, based on the modelling approach presented in [11], a simplified dynamic model for LV microgrids is obtained in a generalized manner. Secondly, the developed system model is constructed in terms of state variables that can be determined from inherent power sharing characteristics of droop control. This eliminates the additional analysis required for determination of equilibrium points of relevant state variables. In this way, the proposed small-signal stability analysis method can be applied to practical LV microgrids in one step.

The rest of the paper is configured as follows; in Section 2, a simplified common microgrid structure is constructed for LV microgrids. Section 3 describes the developed generalized stability analysis method based on the simplified microgrid structure. Section 4 presents the comparison of analysis results with simulation results and effect examination of some critical DG and grid parameters on stability. Conclusion is given in Section 5.

2 Simplified LV microgrid model

Figure 1 presents a generic microgrid structure in radial form. In practical applications, a central controller coordinates the microgrid in a hierarchical manner for optimum

network operations [3, 4]. Intermittent nature of the renewable sources and lack of rotating mass storage of conventional synchronous generators require the use of storage units such as batteries in the microgrid. Then, in the grid connected mode of the microgrid, the coordination problem evolves as the dispatch of DG powers in an optimum manner using appropriate algorithms [18–22]. In this mode, DGs are applied output current based local control strategies to inject the dispatched powers to the grid [2, 23]. In island mode, local control strategy of DGs turns to droop based voltage control strategy for autonomous power sharing. In this mode, power dispatch optimization can be done by updating droop coefficients. Since the stability problem subjected in this paper arises in the island mode, the paper will focus on the island mode of operation, as described in the following parts.

Microgrids are applied mostly in LV distribution networks [1–4]. The islanding switch, shown in Fig. 1, is preferably placed in high voltage side of distribution transformer for safety [24]. The microgrid consists of $N \geq 2$ nodes each of which are represented by a DG and a corresponding load Z_{li} with respective active and reactive powers P_{Li} and Q_{Li} ($i = 1, 2, \ldots, N$). Each DG is connected to the microgrid via a coupling impedance $Z_i := Z_i \theta_i$. In Fig. 1, $\dot{E}_i := E_i \angle \phi_i$ and $\dot{I}_i$ represent complex output voltages and currents of DGs; and $\dot{V}_{Li} := V_{Li} \angle \phi_{Li}$ corresponds to the load voltages. P_i and Q_i denote the active and reactive output powers of DGs and Z_{li} ($i = 1, 2, \ldots, N - 1$) is the impedance of the respective interconnecting line of the LV distribution feeder.

In LV distribution networks, impedances of power lines (Z_{li}) are usually small. On the other hand, a minimum interconnecting line impedance is required between DGs for stable parallel operation, as will be seen in Section 5. For this reason, a significant physical or virtual coupling impedance is intentionally placed at the output of DGs [9, 25, 26]. Therefore, the following assumption can be made for practical LV implementations of microgrids:

$$Z_{li} \approx 0 \qquad i = 1, 2, \ldots, N \tag{1}$$

The assumption in (1) leads the generic LV microgrid model in Fig. 1 to reduce to the simplified common structure given in Fig. 2. In this simplified model, the microgrid loads can be represented by a unified load impedance Z_L with:

$$\begin{cases} P_L = \sum\limits_{i=1}^{N} P_{Li} \\ Q_L = \sum\limits_{i=1}^{N} Q_{Li} \end{cases} \tag{2}$$

where P_L and Q_L are total active and reactive load powers in the microgrid, respectively.
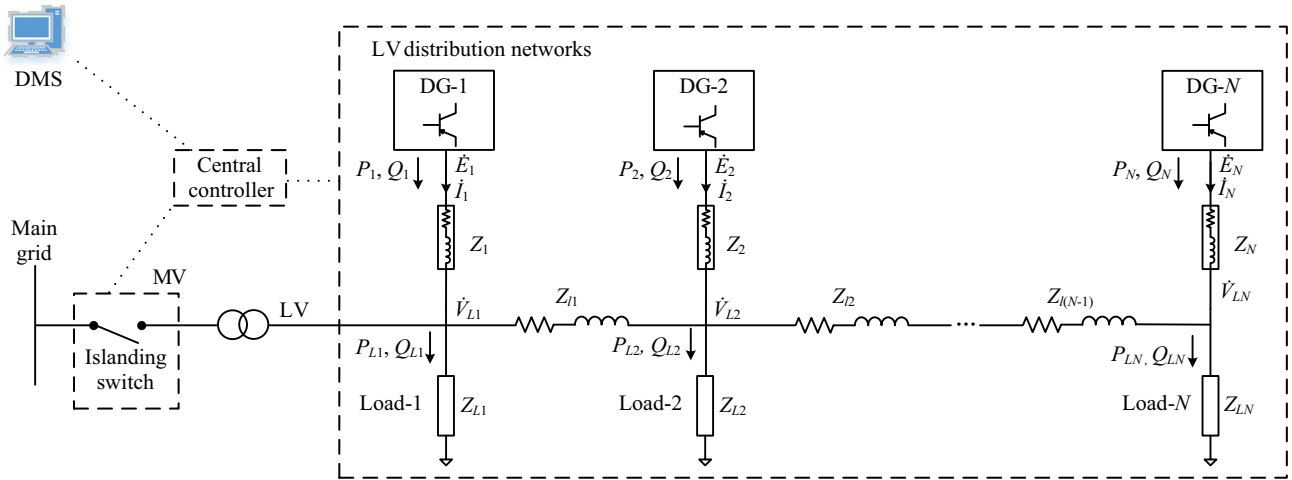
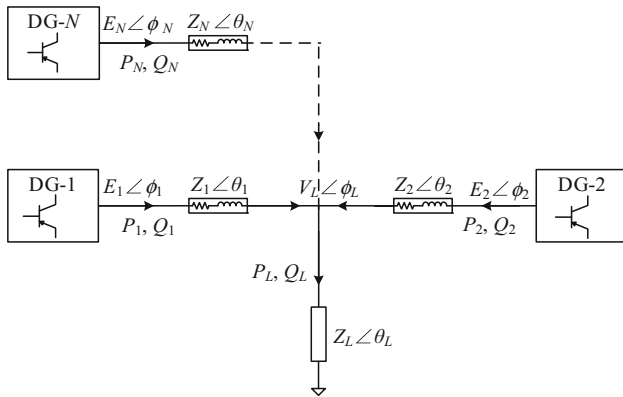**Fig. 1** Microgrid system

Fig. 2 Simplified common LV microgrid model

3 Stability analysis

In this section, equations for the proposed generalized small-signal stability analysis, based on the simplified microgrid model in Fig. 2, are derived. Since the system is non-linear, the analysis will be performed using linearized system equations.

3.1 DG inverter model

Block diagram of a droop controlled DG inverter is shown in Fig. 3. v_g is microgrid voltage; v_o is inverter output voltage (filtered); $v_o{}^*$ is output voltage reference; i_o is inverter output current; v_i is inverter output voltage; $v_i{}^*$ is inverter driver voltage reference; i_f is filter inductance current; $i_f{}^*$ is filter inductance current reference; V_s is inverter DC input voltage; C_s is input Bulk capacitor; m is frequency droop coefficient; and n is voltage droop coefficient. The inverter control structure is composed of an innermost current control loop, an outer voltage control loop and the

outermost droop based power control loop. The common approach for the inner current and voltage controllers is the use of proportional integral (PI) controllers with load compensating feed forward [4, 9, 10, 27]. Since the voltage and current dynamics have no significant impact on the overall system stability, the DG inverters in the microgrid can be treated as ideal voltage sources characterized only by power dynamics dictated by droop control [9–14].

Droop control takes place in power control block in Fig. 3 as:

$$\omega_i = \omega_s - m_i P_{if} \qquad (3)$$

$$E_i = E_s - n_i Q_{if} \qquad (4)$$

where ω_s and E_s are set values for frequency and voltage, corresponding to no-load condition; m_i and n_i denote frequency and amplitude droop coefficients; P_{if} and Q_{if} represent the filtered output powers of DGs, respectively. Dynamic power equations are obtained as follows:

$$\Delta\omega_i = -m_i \frac{w_{fi}}{s + w_{fi}} \Delta P_i \qquad (5)$$

$$\Delta E_i = -n_i \frac{w_{fi}}{s + w_{fi}} \Delta Q_i \qquad (6)$$

where w_{fi} is cut-off frequency of low pass power filters and P_i and Q_i are instantaneous active and reactive output powers of DGs; and Δ denotes small variations of the corresponding state variable. The frequency is related to the phase of the voltage as:

$$\Delta\omega_i = d\Delta\varphi_i/dt \qquad (7)$$

To obtain linearized power expressions for ΔP_i and ΔQ_i, consider a single i^{th} DG in the simplified microgrid model in Fig. 2. The active and reactive powers injected from the ith DG to the common load through corresponding coupling impedance $Z_i \angle \theta_i$ can be expressed as:
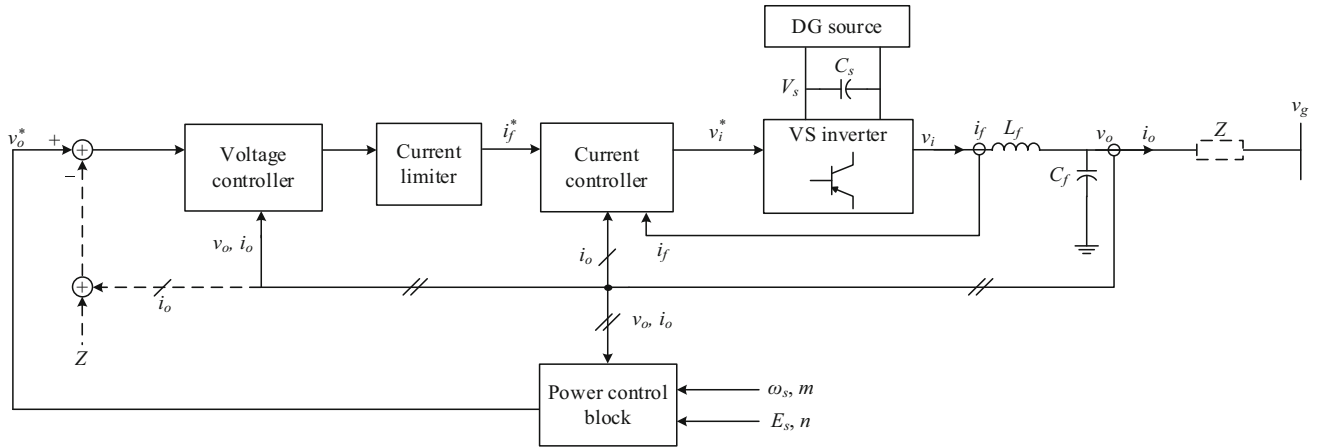
Fig. 3 Block diagram of a droop controlled voltage source inverter

$$P_i = p\left[\frac{E_i V_L}{Z_i}\cos(\theta_i + \varphi_L - \varphi_i) - \frac{V_L^2}{Z_i}\cos\theta_i\right] \qquad (8)$$

$$Q_i = p\left[\frac{E_i V_L}{Z_i}\sin(\theta_i + \varphi_L - \varphi_i) - \frac{V_L^2}{Z_i}\sin\theta_i\right] \qquad (9)$$

where E_i and V_L are the peak magnitudes of DG output voltages and common load voltage respectively; ϕ_i and ϕ_L are phase angles of the corresponding voltages; p is a coefficient related to the phase of the system and is equal to 3/2 for three phase systems and to 1/2 for single phase systems. The linearized power expressions around equilibrium points E_{ie}, ϕ_{ie}, V_{Le}, ϕ_{Le} become:

$$\Delta P_i = k_{i1}\Delta E_i + k_{i2}\Delta\varphi_i + k_{i3}\Delta V_L + k_{i4}\Delta\varphi_L \qquad (10)$$

$$\Delta Q_i = k_{i5}\Delta E_i + k_{i6}\Delta\varphi_i + k_{i7}\Delta V_L + k_{i8}\Delta\varphi_L \qquad (11)$$

where coefficients $k_{ij} \in \mathbb{R}$, ($i = 1, 2, …, N$ and $j = 1, 2, …, 8$) are obtained as:

$$
\begin{cases}
k_{i1} = p\left[\dfrac{V_{Le}}{Z_i}\cos(\theta_i + \varphi_{Le} - \varphi_{ie})\right] \\
k_{i2} = p\left[\dfrac{E_{ie}V_{Le}}{Z_i}\sin(\theta_i + \varphi_{Le} - \varphi_{ie})\right] \\
k_{i3} = p\left[\dfrac{E_{ie}}{Z_i}\cos(\theta_i + \varphi_{Le} - \varphi_{ie}) - \dfrac{2V_{Le}}{Z_i}\cos\theta_i\right] \\
k_{i4} = p\left[\dfrac{-E_{ie}V_{Le}}{Z_i}\sin(\theta_i + \varphi_{Le} - \varphi_{ie})\right] \\
k_{i5} = p\left[\dfrac{V_{Le}}{Z_i}\sin(\theta_i + \varphi_{Le} - \varphi_{ie})\right] \\
k_{i6} = p\left[\dfrac{-E_{ie}V_{Le}}{Z_i}\cos(\theta_i + \varphi_{Le} - \varphi_{ie})\right] \\
k_{i7} = p\left[\dfrac{E_{ie}}{Z_i}\sin(\theta_i + \varphi_{Le} - \varphi_{ie}) - \dfrac{2V_{Le}}{Z_i}\sin\theta_i\right] \\
k_{i8} = p\left[\dfrac{E_{ie}V_{Le}}{Z_i}\cos(\theta_i + \varphi_{Le} - \varphi_{ie})\right]
\end{cases}
\qquad (12)
$$

It should be noted that, when deriving linearized power expressions in (10) and (11), coupling impedances, Z_i is assumed constant and defined as:

$$Z_i = R_i + jX_i \qquad (13)$$

where R_i is the resistance and $X_i = \omega_n L_i$ is the reactance of the ith coupling impedance defined for the nominal angular frequency, ω_n of the microgrid. Note that the static coupling impedance model is claimed to decrease the accuracy of the analysis and alternatively a dynamic coupling approach has been proposed in [12], which will be discussed again in Section 4.

The coefficients given in (12) have the usual structure with equilibrium point values of voltage amplitudes and voltage phase angles. These equilibrium values are needed for the analysis to be performed. But the voltage phase angles are difficult to estimate and additional analysis is required to obtain them. Dynamic simulations or load flow analysis are the common tools used in the literature to obtain these equilibrium values. Fortunately, by comparing the coefficients in (12) with power expressions in (8) and (9), the coefficients can be obtained equivalently as:

$$
\begin{cases}
k_{i1} = \dfrac{P_{ie}}{E_{ie}} + p\dfrac{V_{Le}^2}{Z_i E_{ie}}\cos\theta_i \\
k_{i2} = Q_{ie} + p\dfrac{V_{Le}^2}{Z_i}\sin\theta_i \\
k_{i3} = \dfrac{P_{ie}}{V_{Le}} - p\dfrac{V_{Le}}{Z_i}\cos\theta_i \\
k_{i4} = -Q_{ie} - p\dfrac{V_{Le}^2}{Z_i}\sin\theta_i \\
k_{i5} = \dfrac{Q_{ie}}{E_{ie}} + p\dfrac{V_{Le}^2}{Z_i E_{ie}}\sin\theta_i \\
k_{i6} = -P_{ie} - p\dfrac{V_{Le}^2}{Z_i}\cos\theta_i \\
k_{i7} = \dfrac{Q_{ie}}{V_{Le}} - p\dfrac{V_{Le}}{Z_i}\sin\theta_i \\
k_{i8} = P_{ie} + p\dfrac{V_{Le}^2}{Z_i}\cos\theta_i
\end{cases}
\qquad (14)
$$

The coefficients in (14) require only steady-state loadings and steady-state voltage magnitudes of DG inverter outputs and loads. The inherent power sharing property of droop control for active power and derived expression for reactive power sharing below provide approximate ways to obtain these parameters analytically. Besides, for LV networks, nominal operating voltage of the microgrid can be assigned to all steady-state voltage magnitudes.

Active power sharing: In steady state, the frequency of the microgrid is the same at all nodes. Then, from (3), for the same frequency set point ω_s for all DGs, the total active power in the microgrid is shared between the DG inverters according to the expression below:

$$m_1 P_{1e} = m_2 P_{2e} = \ldots = m_i P_{ie} \tag{15}$$

With the assumption in (1), the total active power loading of the microgrid given in (2) corresponds to the total output powers of DGs. Using (15) active power of each DG can be analytically calculated.

Reactive power sharing: Reactive power sharing between DGs is not only dictated by amplitude droop coefficient n but also by interconnecting line impedances [25]. Based on the characteristics of LV distribution networks, the following assumption for the amplitudes of the node voltages can be made:

$$E_{ie} \approx V_{Le} \qquad i = 1, 2, .., N \tag{16}$$

Then from (8) and using (16),

$$\theta_i + \varphi_{Le} - \varphi_{ie} = \delta_{ie} = a \cos\left(\frac{P_{ie} Z_i}{p V_{Le}^2} + \cos \theta_i\right) \tag{17}$$

Substitute (17) and (4) into (9):

$$Q_{ie} = p \left[\frac{(E_s - n Q_{ie}) V_{Le}}{Z_i} \sin \delta_{ie} - \frac{V_{Le}^2}{Z_i} \sin \theta_i\right] \tag{18}$$

Rearrange (18), the expression of reactive power sharing can be obtained as:

$$Q_{ie}\left(\frac{Z_i}{p V_{Le} \sin \delta_{ie}} + n_i\right) + V_{Le}\frac{\sin \theta_i}{\sin \delta_{ie}} = c \tag{19}$$

where $c = E_s$ is a constant, and δ_{ie} is defined as:

$$\delta_{ie} = a \cos\left(\frac{P_{ie} Z_i}{p V_{Le}^2} + \cos\theta_i\right) \tag{20}$$

Using (19), the total steady-state reactive power loading in the microgrid can be distributed to DGs in a similar manner as in the case of active power.

3.2 Load equations

Average active and reactive load powers of the unified RL load in Fig. 2 can be expressed as:

$$\begin{cases} P_L = \dfrac{V_L^2}{Z_L} \cos \theta_L \\[3mm] Q_L = \dfrac{V_L^2}{Z_L} \sin \theta_L \end{cases} \tag{21}$$

where $Z_L \angle \theta_L$ is the complex impedance of the unified load in polar form. Linearization of load power expressions leads to:

$$\begin{cases} \Delta P_L = \dfrac{2 V_{Le}}{Z_L} \cos \theta_L \Delta V_L \\[3mm] \Delta Q_L = \dfrac{2 V_{Le}}{Z_L} \sin \theta_L \Delta V_L \end{cases} \tag{22}$$

Comparing linearized equations in (22) with power expressions in (21), the linearized load power expressions can be expressed in terms of steady-state load powers as:

$$\begin{cases} \Delta P_L = \dfrac{2 P_{Le}}{V_{Le}} \Delta V_L \\[3mm] \Delta Q_L = \dfrac{2 Q_{Le}}{V_{Le}} \Delta V_L \end{cases} \tag{23}$$

3.3 Combined microgrid equations

In terms of power dynamics, a droop controlled DG inverter is a 3rd order system based on dynamics of two first order low pass power filters and angular frequency. If state variables are chosen as $\Delta\omega_i$, ΔE_i and $\Delta\varphi_i$, the small-signal dynamical model of the single i^{th} DG inverter can be obtained from (5)–(7) as:

$$\begin{cases} \Delta\dot{\omega}_i = -w_{fi}\Delta\omega_i + k'_{i1}\Delta E_i + k'_{i2}\Delta\varphi_i + k'_{i3}\Delta V_L + k'_{i4}\Delta\varphi_L \\ \Delta\dot{E}_i = k'_{i5}\Delta E_i + k'_{i6}\Delta\varphi_i + k'_{i7}\Delta V_L + k'_{i8}\Delta\varphi_L \\ \Delta\dot{\varphi}_i = \Delta\omega_i \end{cases} \tag{24}$$

where $k'_{i1} = -m_i w_{fi} k_{i1}$; $k'_{i2} = -m_i w_{fi} k_{i2}$; $k'_{i3} = -m_i w_{fi} k_{i3}$; $k'_{i4} = -m_i w_{fi} k_{i4}$; $k'_{i5} = -w_{fi} - n_i w_{fi} k_{i5}$; $k'_{i6} = -n_i w_{fi} k_{i6}$; $k'_{i7} = -n_i w_{fi} k_{i7}$; $k'_{i8} = -n_i w_{fi} k_{i8}$.

In (24), non-state variables ΔV_L and $\Delta\varphi_L$ can be reduced from the equations by using the equality of powers at load bus as:

$$\begin{cases} \displaystyle\sum_{i=1}^{N} \Delta P_i = \Delta P_L \\[3mm] \displaystyle\sum_{i=1}^{N} \Delta Q_i = \Delta Q_L \end{cases} \tag{25}$$

Substitute (10), (11) and (23) into (25), we can obtain:

$$\begin{bmatrix} \Delta V_L \\ \Delta\varphi_L \end{bmatrix} = \boldsymbol{\alpha}^{-1} \boldsymbol{\beta} \begin{bmatrix} \Delta E_i \\ \Delta\varphi_i \\ \Delta\omega_i \end{bmatrix}_{3N\times 1} \tag{26}$$

where $\boldsymbol{\alpha}$ is a 2×2 matrix defined as:

$$\boldsymbol{\alpha} = \begin{bmatrix} \dfrac{2P_{Le}}{V_{Le}} - \sum k_{i3} & -\sum k_{i4} \\ \dfrac{2Q_{Le}}{V_{Le}} - \sum k_{i7} & -\sum k_{i8} \end{bmatrix} \qquad (27)$$

and $\boldsymbol{\beta}$ is a $2 \times 3N$ matrix defined as:

$$\boldsymbol{\beta} = \begin{bmatrix} k_{i1}\dots & k_{i2}\dots & 0\dots \\ k_{i5}\dots & k_{i6}\dots & 0\dots \end{bmatrix} \qquad (28)$$

Substitute (26) into (24), the following homogeneous equation in state-space form is obtained:

$$\begin{bmatrix} \Delta\dot{E}_i \\ \Delta\dot{\varphi}_i \\ \Delta\dot{\omega}_i \end{bmatrix} = \underbrace{\begin{bmatrix} \boldsymbol{a} \\ \boldsymbol{b} \\ \boldsymbol{c} \end{bmatrix}}_{A} \begin{bmatrix} \Delta E_i \\ \Delta\varphi_i \\ \Delta\omega_i \end{bmatrix} \qquad (29)$$

where $\boldsymbol{a}, \boldsymbol{b}, \boldsymbol{c}$ are defined as:

$$\begin{cases} \boldsymbol{a} = \begin{bmatrix} k'_{15} & \dots & 0 & k'_{16} & \dots & 0 & 0 & \dots & 0 \\ \vdots & & \vdots & \vdots & & \vdots & \vdots & & \vdots \\ 0 & \dots & k'_{N5} & 0 & \dots & k'_{N6} & 0 & \dots & 0 \end{bmatrix} + \\ \qquad \begin{bmatrix} k'_{17} & k'_{18} \\ \vdots & \vdots \\ k'_{N7} & k'_{N8} \end{bmatrix} \boldsymbol{\alpha}^{-1}\boldsymbol{\beta} \\ \boldsymbol{b} = \begin{bmatrix} \boldsymbol{0} & \boldsymbol{0} & \boldsymbol{I} \end{bmatrix} \\ \boldsymbol{c} = \begin{bmatrix} k'_{11} & \dots & 0 & k'_{12} & \dots & 0 & -w_{f1} & \dots & 0 \\ \vdots & & \vdots & \vdots & & \vdots & \vdots & & \vdots \\ 0 & \dots & k'_{N1} & 0 & \dots & k'_{N2} & 0 & \dots & -w_{fN} \end{bmatrix} + \\ \qquad \begin{bmatrix} k'_{12} & k'_{14} \\ \vdots & \vdots \\ k'_{N3} & k'_{N4} \end{bmatrix} \boldsymbol{\alpha}^{-1}\boldsymbol{\beta} \end{cases}$$

$$(30)$$

Fig. 4 Structure of test microgrid

In (29) and (30), dimension of A matrix is $3N$ and sub-matrices $\boldsymbol{a}, \boldsymbol{b}, \boldsymbol{c}$ has a dimension of $N \times 3N$. $\boldsymbol{I}$ is an identity matrix and $\boldsymbol{0}$ is a null matrix with the dimension of $N \times N$.

4 Analysis results

Developed stability analysis method has been applied to a test microgrid with two DG-load pair connected with an interconnecting line, as shown in Fig. 4. The test grid has three-phase, 60 Hz and 130 V nominal phase-neutral voltage. Parameters of inverters and corresponding coupling impedances, interconnecting line and loads are given in Table 1. For the value of the interconnecting line impedance Z_l, impedance of the main distribution feeder of CIGRE network has been chosen [28]. The rated power of DG-1 is devised to be the half of DG-2, then the droop coefficients are set as $m_1 = 2m_2 = 0.005$ and $n_1 = 2n_2 = 0.01$. The simulations have been performed using MATLAB-Simulink. In the simulations, the actual test microgrid in Fig. 4 has been used. The analysis has been applied to the simplified model of the test structure by neglecting interconnecting line impedance. For the analysis, the system state matrix A given in (29) has been used, from which eigenvalues λ_k, $(k = 1,2,\dots,3N)$ of the system can be obtained.

Case 1: In the first case, the simulation has been performed for the given microgrid parameters above. The equilibrium points of the relevant parameters, obtained

Table 1 Parameters of test microgrid

Type	Parameter	Value	Unit
DG inverters and coupling impedances	Switching frequency f_s	10	kHz
	Output filter inductance L_f	1.84	mH
	Output filter resistance r_f	0.11	Ω
	Output filter capacitance C_f	30	μF
	Cut-off frequency of power filters w_f	31.85	rad/s
	Voltage frequency set value ω_s	380	rad/s
	Voltage amplitude set value E_s	132	V
	DC input voltage V_s	310	V
	Inductance of Z_1	0.77	mH
	Resistance of Z_1	0.11	Ω
	Inductance of Z_2	1.57	mH
	Resistance of Z_2	0.19	Ω
Interconnection line	Line impedance Z_l	81.5+j68	mΩ
Loads	Impedance of load-1 Z_{L1}	47+j56.5	Ω
	Impedance of load-2 Z_{L2}	47	Ω
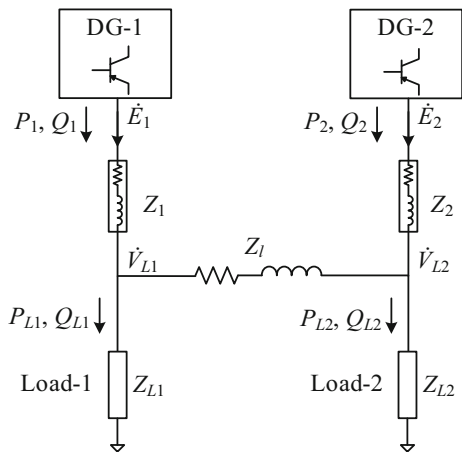
from the simulation, are given in Table 2. When the analysis is performed using the actual equilibrium points given in Table 2. The eigenvalues of the system are obtained from (30) as: $\lambda_1 = 0$, $\lambda_2 = -31.85$, $\lambda_3 = -32.3$, $\lambda_4 = -131.4$, $\lambda_5 = -14.1 + j79.9$, and $\lambda_6 = -14.1 - j79.9$.

On the other hand, for 130 V phase-neutral nominal grid voltage, and from (15) and (19) the individual active and reactive DG powers are calculated as $2P_1 = P_2 = 506.6$ W, $Q_1 = 130$ var, $Q_2 = 135$ var. The corresponding system eigenvalues are obtained as: $\lambda_1 = 0$, $\lambda_2 = -31.85$, $\lambda_3 = -32.3$, $\lambda_4 = -130.7$, $\lambda_5 = -14.2 + j79.4$, and $\lambda_6 = -14.2 - j79.4$.

As seen from both results, use of approximate values for equilibrium points of power and voltages does not make significant change in the system eigenvalues. Complex eigenvalues with negative real parts state that the system has a stable and oscillatory response. The zero eigenvalue points out the existence of multiple equilibrium points for voltage phase angles. Note that the behavior of the system is dictated by differences of voltage phase angles. Figures 5 and 6 present simulation and analysis results for the frequency waveforms of the inverters in the test microgrid. The analysis results have been obtained with both actual and approximate (simplified analysis) equilibrium point values on the same plot. The frequency waveforms also indicates that the developed analysis model represents the microgrid system quite well for the given condition. However, parameter selection for a system is dictated mainly by instability conditions and a successful analysis tool should be accurate in determining instability boundaries. Therefore, the next test condition has been selected around an instability boundary.

Case 2: A boundary of instability emerges in the simulations for the frequency droop coefficient values of $m_1 = 2m_2 = 0.015$, while the other parameters are kept the same. For this condition, the simplified analysis method results in the system eigenvalues: $\lambda_1 = 0$, $\lambda_2 = -31.85$,
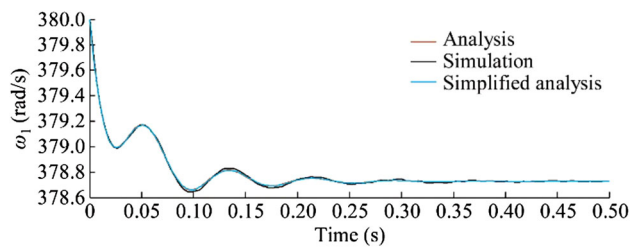
Table 2 Equilibrium points for Case 1

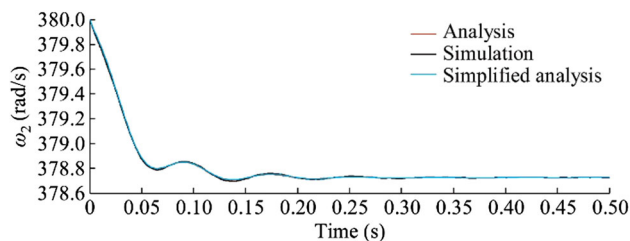| Parameter	Value
E_1	130.5
E_2	131.0
V_{L1}	130.0
V_{L2}	130.2
P_1	255.0
P_2	510.0
Q_1	131.0
Q_2	142.0

Fig. 5 Frequency waveforms of DG-1 for Case 1

Fig. 6 Frequency waveforms of DG-2 for Case 1

$\lambda_3 = -32.3$, $\lambda_4 = -134.2$, $\lambda_5 = -12.7 + j138.6$, and $\lambda_6 = -12.7 - j138.6$.

The negative real parts in the analysis results above, however, point out a stable system. The simulation and analysis results for the frequency variation of DG-1 is shown in Fig. 7. This result means that as the conditions approach the stability boundaries of the system the accuracy of the analysis reduces. The same discrepancy has been observed in the literature and there exist two claims for it. In [11], the reduction of analysis accuracy with increasing m is devoted to the reduction of accuracy of the small-signal model due to the increased deviations of initial points of frequencies from equilibrium points. In [12], it is reasoned by no inclusion of inductive coupling dynamics in the analysis. To investigate the effect of inductive couplings, another instability boundary has been searched in the simulations by introducing pure resistive couplings between the inverters.

Case 3: For resistive couplings, an instability boundary is observed when Z_1 is set to 1.2 Ω and Z_2 is set to 1.8 Ω while keeping the remaining parameters the same as in Case 1. When the analysis is performed for this condition,
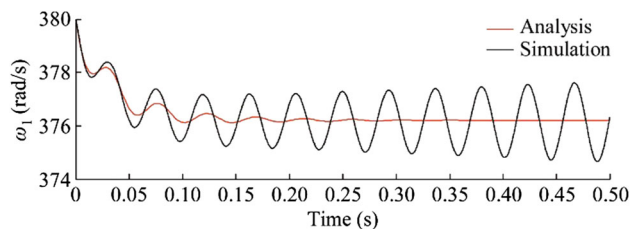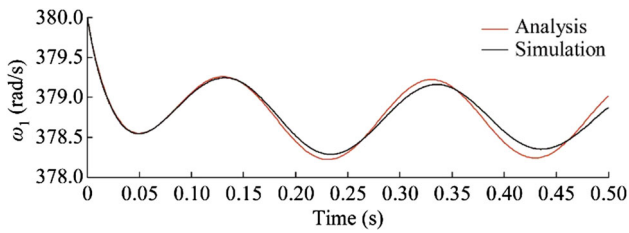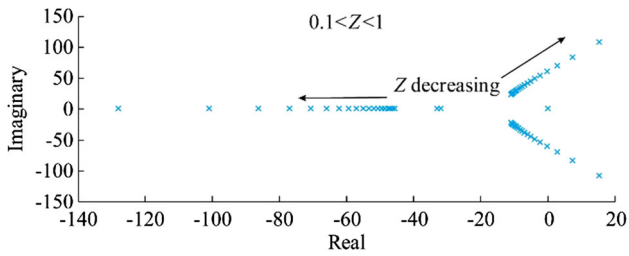

Fig. 7 Frequency waveforms of DG-1 for Case 2
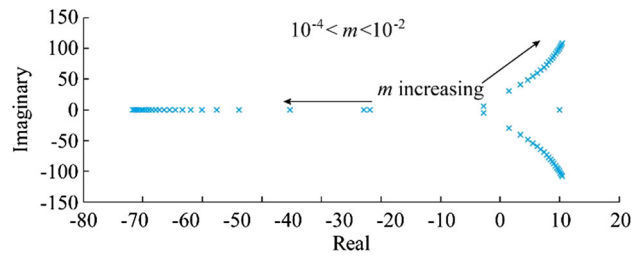
Fig. 8 Frequency waveforms of DG-1 for Case 3

Fig. 9 Trajectories of system eigenvalues for decreasing Z ($P_i = 5$ kW, $Q_i = 3$ kvar, $m_i = 0.001$, $n_i = 0.001$, $\theta_i = \pi/8$, $V_L = 180$ V, $w_{fi} = 31.85$ rad/s)

Fig. 10 Trajectories of system eigenvalues for increasing m ($P_i = 5$ kW, $Q_i = 3$ kvar, $n_i = 0.001$, $Z_i = 0.5$, $\theta_i = \pi/8$, $V_L = 180$ V, $w_{fi} = 31.85$ rad/s)

Fig. 11 Trajectories of system eigenvalues for increasing grid voltage ($P_i = 5$ kW, $Q_i = 3$ kvar, $m_i = 0.001$, $n_i = 0.001$, $Z_i = 0.5$, $\theta_i = \pi/8$, $w_{fi} = 31.85$ rad/s)
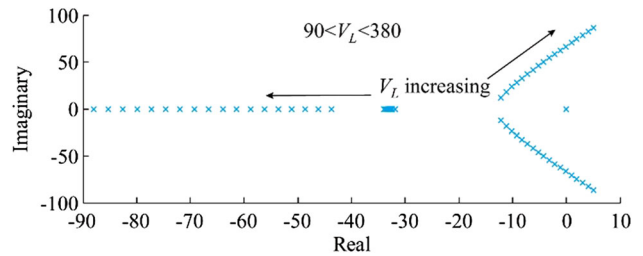
the system eigenvalues are obtained as: $\lambda_1 = 0$, $\lambda_2 = -31.85$, $\lambda_3 = -32.3$, $\lambda_4 = -63.9$, $\lambda_5 = -0.16 + j31.6$, and $\lambda_6 = -0.16 - j31.6$.

The corresponding simulation and analysis results for DG-1 inverter frequency are presented in Fig. 8. As seen from the results, in case of resistive couplings between the inverters, the proposed analysis method accurately predicts the instability boundaries. Note that the coupling impedances at the outputs of DGs can be virtually implemented. In addition, resistive grids have respective advantages compared to inductive grids [25, 29]. Therefore, for microgrids with resistive coupling impedances, the proposed analysis method can be effectively used in determining system parameters.

To analyze the effect of system parameters on stability a parametric stability analysis can be performed. The concerned parameter can be varied while the others are kept constant and the analysis is repeated for each value of the varying parameter. The simple structure of the proposed method facilitates this process. Figure 9 shows trace of system eigenvalues for the variation of coupling impedance amplitude Z while the other parameters are kept constant. The microgrid system requires a minimum amplitude for the coupling impedances ($Z \approx 0.4$ for given conditions) for stable operation. This result reinforces the assumption in (1). Another result, consistent with the complete model in [9], is presented in Fig. 10. It states that the increasing power droop coefficient m deteriorates the system stability. An interesting result is observed in case of variation of the grid voltage. It is observed that the increasing grid voltage deteriorates the system stability, as shown in Fig. 11. This result dictates inclusion of grid voltage as a critical design parameter in terms of system stability.

5 Conclusion

This paper presents a simplified stability analysis method for island mode operation of inverter-based LV microgrids. The analysis method is based on the characteristics of LV distribution networks.

Analysis and simulation results have shown that the stability of island mode microgrids are not sensitive to small variations of grid parameters such as node voltage amplitudes and DG powers. Then, by approximately obtaining the parameters of linearized power expressions in terms of these grid parameters, additional prerequisite analyses to determine equilibrium points of the state variables have been eliminated, which considerably facilitates the analysis. Analysis results have shown that the stability of microgrid is highly sensitive to interconnecting line impedances between DGs. It has been observed that inductive coupling dynamics lead the analysis results to deviate around the instability boundaries. However, the analysis method can successfully predict the instability boundaries for resistive networks.

Springer

References

[1] Arulampalam A, Barnes M, Engler A et al (2004) Control of power electronic interfaces in distributed generation microgrids. Int J Electron 91(9):503–523

[2] Lopes JAP, Moreira CL, Madureira AG (2006) Defining control strategies for microgrids islanded operation. IEEE Trans Power Syst 21(2):916–924

[3] Guerrero JM, Chandorkar M, Lee TL et al (2013) Advanced control architectures for intelligent microgrids-Part I: decentralized and hierarchical control. IEEE Trans Ind Electron 60(4):1254–1262

[4] Olivares DE, Mehrizi-Sani A, Etemadi AH et al (2014) Trends in microgrid control. IEEE Trans Smart Grid 5(4):1905–1919

[5] Majumder R, Bag G (2014) Parallel operation of converter interfaced multiple microgrids. Electr Power Energy Syst 55(2):486–496

[6] Quesada J, Sebastian R, Castro M et al (2014) Control of inverters in a low voltage microgrid with distributed battery energy storage-Part I: primary control. Electr Power Syst Res 114(3):126–135

[7] Hassan MA, Abido MA (2014) Real time implementation and optimal design of autonomous microgrids. Electr Power Syst Res 109(109):118–127

[8] Kundur P (1994) Small-signal stability. In: Balu NJ, Lauby MG (eds) Power systems stability and control. McGraw-Hill, New York, pp 699–822

[9] Pogaku N, Prodanovic M, Green TC (2007) Modeling, analysis and testing of autonomous operation of an inverter-based microgrid. IEEE Trans Power Electron 22(2):613–625

[10] Mohamed YARI, Saadany EFE (2008) Adaptive decentralized droop controller to preserve power sharing stability of paralleled inverters in distributed generation microgrids. IEEE Trans Power Electron 23(6):2806–2816

[11] Cohelho EAA, Cortizo PC, Garcia PFD (2002) Small-signal stability for parallel-connected inverters in stand-alone AC supply systems. IEEE Trans Ind Appl 38(2):533–542

[12] Guo X, Lu Z, Wang B et al (2014) Dynamic phasors-based modelling and stability analysis of droop-controlled inverters for microgrid applications. IEEE Trans Smart Grid 5(6):2980–2987

[13] Mariani V, Vasca F, Vasquez J et al (2015) Model order reductions for stability analysis of islanded microgrids with droop control. IEEE Trans Ind Electron 62(7):4344–4354

[14] Iyer SV, Belur MN, Chandorkar MC (2010) A generalized computational method to determine stability of a multi-inverter microgrid. IEEE Trans Power Electron 25(9):2420–2432

[15] Luo L, Dhople SV (2014) Spatiotemporal model reduction of inverter based islanded microgrids. IEEE Trans Energy Convers 29(4):823–832

[16] Rasheduzzaman M, Mueller JA, Kimball JW (2015) Reduced-order small-signal model of microgrid systems. IEEE Trans Sustain Energy 6(4):1292–1305

[17] Nikolakakos IP, Zeineldin HH, Moursi MSE et al (2018) Reduced-order model for inter-inverter oscillations in islanded droop-controlled microgrids. IEEE Trans Smart Grid 9(5):4953–4963

[18] Reddy SS, Momoh JA (2015) Realistic and transparent optimum scheduling strategy for hybrid power system. IEEE Trans Smart Grid 6(6):3114–3125

[19] Reddy SS, Bijwe PR, Abhyankar AR (2015) Optimal posturing in day-ahead market clearing for uncertainties considering anticipated real time adjustment costs. IEEE Syst J 9(1):177–190

[20] Reddy SS, Bijwe PR, Abhyankar AR (2015) Joint energy and spinning reserves market clearing for wind-thermal power system incorporating wind generation and load forecast uncertainties. IEEE Syst J 9(1):152–164

[21] Reddy SS (2017) Optimal power flow with renewable energy resources including storage. Electr Eng 99(2):685–695

[22] Reddy SS, Park JY, Jung CM (2016) Optimal operation of microgrid using hybrid differential evolution and harmony search algorithm. Front Energy 10(3):355–362

[23] Dag B, Boynuegri AR, Ates Y et al (2017) Static modelling of microgrids for load flow and fault analysis. IEEE Trans Power Syst 32(3):1990–2000

[24] Jayawarna N, Jenkins N, Barnes M et al (2006) Safety analysis of a microgrid. In: Proceedings of 2005 international conference on future power systems, Amsterdam, Netherlands, 18 November 2005, 7pp

[25] Zhong QC (2013) Robust droop controller for accurate proportional load sharing among inverters operated in parallel. IEEE Trans Ind Electron 60(4):1281–1290

[26] Guerrero JM, Matas J, Vicuna LG et al (2006) Wireless-control strategy for parallel operation of distributed-generation inverters. IEEE Trans Ind Electron 53(5):1461–1470

[27] Delghavi MB, Yazdani A (2011) An adaptive feedforward compensation for stability enhancement in droop-controlled inverter-based microgrids. IEEE Trans Power Deliv 26(3):1764–1773

[28] Bhutto G, Bak-Jensen B, Bak C et al (2013) Protection of low voltage CIGRE distribution network. Smart Grid Renew Energy 4:489–500

[29] Guerrero JM, Hang L, Uceda J (2008) Control of distributed uninterruptible power supply systems. IEEE Trans Ind Electron 55(8):2845–2859

Bülent DAĞ received the B.Sc. and M.Sc. degrees in Electrical and Electronics Engineering from Middle East Technical University, Ankara, Turkey, in 1998 and 2002, respectively, and the Ph.D. degree in Electrical and Electronics Engineering from Gazi University, Ankara, Turkey, in 2015. In 2001, he worked as a scholarship researcher at University of Picardie, Amiens, France, and in 2003, as a research assistant at Technical University of Eindhoven, Netherlands. Since 2006, he has been working as a researcher with The Scientific and Technological Research Council of Turkey. His research interests include electrical machines, distributed-generation sources with power electronics interfaces, and satellite power systems.

M. Timur AYDEMIR received his B.Sc. degree in 1983 and M.Sc. degree in 1985, both in Electrical Engineering from Karadeniz (Blacksea) Technical University, where he also worked as a research assistant. In 1988, he won a scholarship from the Ministry of Education of Turkey for Ph.D. education in the USA. He received his Ph.D. degree from the University of Wisconsin-Madison in 1995. Since then he has been working at Gazi University, Faculty of Engineering, Department of Electrical and Electronic Engineering. During 2001-02 school year, he was a visiting researcher at the University of Wisconsin-Madison on Fulbright Scholarship. He is also the vice-director of Gazi University Clean Energy Research and Application Center. His areas of interest include power electronics, electrical machines and drives, and renewable energy systems.

STATE GRID
STATE GRID ELECTRIC POWER RESEARCH INSTITUTE